Received: 6 December 2023 | Revised: 9 March 2024 | Accepted: 2 April 2024

DOI: 10.1111/1440-1681.13865

ORIGINAL ARTICLE

CEPP Clinical and Experimental Pharmacology and Physiology WILEY

# In vitro effects and mathematical modelling of CTCE-9908 (a chemokine receptor 4 antagonist) on melanoma cell survival

Charlise Basson[1] | Avulundiah Edwin Phiri[2] | Manjunath Gandhi[2] | Roumen Anguelov[2] | June Cheptoo Serem[3] | Priyesh Bipath[1] | Yvette Nkondo Hlophe[1]

[1]Department of Physiology, University of Pretoria, Pretoria, South Africa

[2]Department of Mathematics, Faculty of Natural and Agricultural Sciences, University of Pretoria, Pretoria, South Africa

[3]Department of Anatomy, University of Pretoria, Pretoria, South Africa

**Correspondence**
Yvette Nkondo Hlophe, Department of Physiology, Faculty of Health Sciences, School of Medicine, University of Pretoria, Private Bag X323, Gezina, Pretoria, Gauteng 0031, South Africa.
Email: yvette.hlophe@up.ac.za

**Funding information**
National Research Foundation; Struwig-Germeshuysen Kankernavorsingstrust; School of Medicine Research Committee (RESCOM); Research Development Program

## Abstract

CTCE-9908, a CXC chemokine receptor 4 (CXCR4) antagonist, prevents CXCR4 phosphorylation and inhibits the interaction with chemokine ligand 12 (CXCL12) and downstream signalling pathways associated with metastasis. This study evaluated the in vitro effects of CTCE-9908 on B16 F10 melanoma cells with the use of mathematical modelling. Crystal violet staining was used to construct a mathematical model of CTCE-9908 B16 F10 (melanoma) and RAW 264.7 (non-cancerous macrophage) cell lines on cell viability to predict the half-maximal inhibitory concentration ($IC_{50}$). Morphological changes were assessed using transmission electron microscopy. Flow cytometry was used to assess changes in cell cycle distribution, apoptosis via caspase-3, cell survival via extracellular signal-regulated kinase1/2 activation, CXCR4 activation and CXCL12 expression. Mathematical modelling predicted $IC_{50}$ values from 0 to 100 h. At $IC_{50}$, similar cytotoxicity between the two cell lines and ultrastructural morphological changes indicative of cell death were observed. At a concentration 10 times lower than $IC_{50}$, CTCE-9908 induced inhibition of cell survival ($p = 0.0133$) in B16 F10 cells but did not affect caspase-3 or cell cycle distribution in either cell line. This study predicts CTCE-9908 $IC_{50}$ values at various time points using mathematical modelling, revealing cytotoxicity in melanoma and non-cancerous cells. CTCE-9908 significantly inhibited melanoma cell survival at a concentration 10 times lower than the $IC_{50}$ in B16 F10 cells but not RAW 264.7 cells. However, CTCE-9908 did not affect CXCR4 phosphorylation, apoptosis,\ or cell cycle distribution in either cell line.

**KEYWORDS**
cell survival, CTCE-9908, CXCL12, CXCR4, mathematical modelling, melanoma

## 1 | INTRODUCTION

Melanoma is a relentless form of cancer and remains a governing concern due to its ability to metastasise.[1] The estimated 1-year survival rate of melanoma patients with stage IV melanoma with metastasis to (1) distantthe n skin is approximately 59%, (2) the lungs is approximately 57%, and (3) to other visceral sites is 41%.[2] To date, melanoma is responsible for more than 80% of skin cancer-related deaths.[3]

Despite major advances in the treatment of melanoma patients, no cure exists for the treatment of metastatic melanoma.[4] Therefore, the incidence and mortality rate remains alarmingly high, emphasising the need for novel treatment strategies to inhibit melanoma metastasis.[5]

It is well known that chemokines are major contributors to melanoma progression and metastasis.[1,6] Chemokines promote metastasis of chemokine-expressing cancer cells to organs that overexpress the corresponding chemokine ligand.[7] Among these chemokines, CXC chemokine receptor 4 (CXCR4) is overexpressed in melanoma and, therefore, represents an attractive target to inhibit melanoma metastasis.[8] CXCR4 is a G-protein coupled receptor,[9] which binds to its cognate chemokine ligand, namely CXC chemokine ligand 12 (CXCL12),[7] and activates the CXCR4/CXCL12 axis, leading to the activation of several downstream signalling cascades, including the mitogen-activated protein kinase (MAPK), phosphoinositide 3-kinase/ protein kinase B (PI3K/AKT), phospholipase C (PLC) and Ras homologue gene member A (RhoA) pathway.[1] The activation of these pathways contributes to melanoma metastasis by promoting tumour cell migration, survival, adhesion and proliferation.[1]

A known CXCR4 inhibitor, CTCE-9908, was granted approval by the Food and Drug Administration (FDA) for the treatment of osteogenic sarcoma.[1] CTCE-9908 is a peptide analogue of CXCL12 and contains an altered NH2-terminal sequence.[10] CTCE-9908 inhibits CXCR4 by competitively binding to it and, therefore, disrupting receptor phosphorylation.[6,10] The latter might lead to the inactivation of CXCR4/CXCL12-associated downstream signalling pathways to inhibit cell migration, adhesion and proliferation.[1]

This study, therefore, aimed to elucidate the effects of altered chemokine activation by CTCE-9908 on cell proliferation, morphology, survival, apoptosis and cell cycle in B16 F10 melanoma and RAW 264.7 cells in vitro and proposed a mathematical model for the prediction of CXCR4-inhibition on cell proliferation at increased time (*t*) points ranging from 0 to 100 h.

## 2 | RESULTS

### 2.1 | Cytotoxicity with crystal violet staining

B16 F10, as well as RAW 264.7 cells, were exposed to a CXCR4 inhibitor (CTCE-9908) in a range (0–0.051 mM) for 24, 48 and 72 h. In both cell lines, CTCE-9908 did not display statistically significant cytotoxic effects (Figure 1A,B).

The increased CTCE-9908 concentrations (0–0.31 mM) at 48 hours showed that CTCE-9908 induced significant cytotoxic effects at 0.31 mM (Figure 2).

In the B16 F10 cell line, at higher CTCE-9908 concentrations at 48 h, an $IC_{50}$ of 0.53 mM was calculated using GraphPad Prism. In RAW 264.7 cells, an $IC_{50}$ of 0.48 mM was calculated. The $IC_{50}$ values of the B16 F10 and RAW 264.7 cell lines were tested for normality with the Shapiro–Wilk test and then compared using an ANOVA test on GraphPad Prism. The test confirmed that the $IC_{50}$ values were statistically similar, with a *p*-value of 0.79.

### 2.2 | Mathematical modelling of CTCE-9908 inhibition using nonuniformly distributed data

Using the data derived from lower (0.013–0.051 mM) CTCE-9908 concentrations, the cell viability function was obtained using a two-parameter cell viability model, previously determined by our research group for another compound that shows anti-cancer activity, namely L-kynurenine.[11] However, no significant inhibition of cell proliferation was observed at these CTCE-9908 concentrations. After observing the lack of cytotoxicity in B16 F10 cells at these concentrations, higher concentrations of CTCE-9908 were added at 48 h (0.1, 0.31 mM), as a previous study by Kim et al. demonstrated that CTCE-9908 at 100 μg/mL only started to show growth inhibition in osteosarcoma cells after 25 h of treatment.[12] The dynamics of CTCE-9908 concentration versus time for both lower (at 24, 48 and 72 h) and

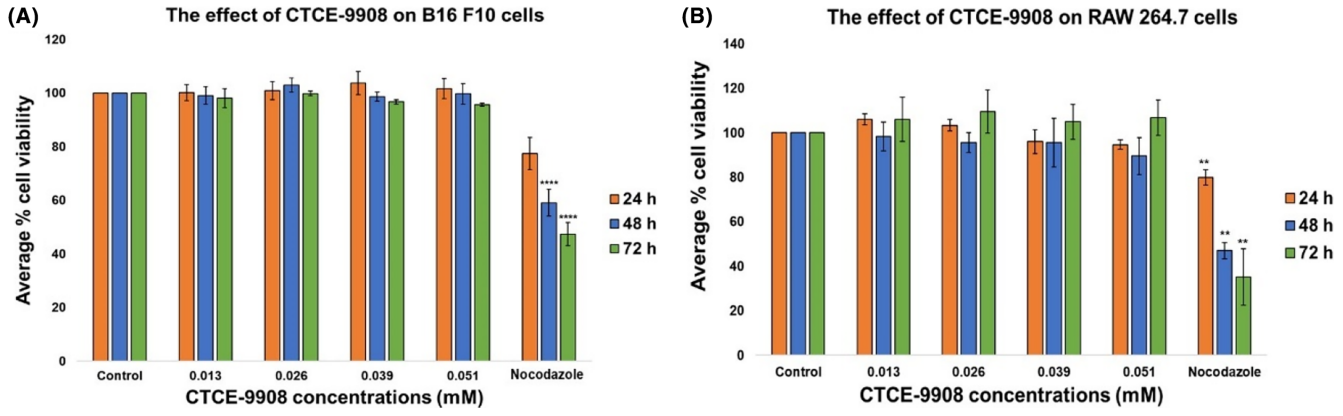


**FIGURE 1** The effect of CTCE-9908 on cell viability of (A) B16 F10 and (B) RAW 264.7 cells at 24, 48 and 72 h in vitro. Cell viability values are expressed as the percentage of viable cells relative to CCM: $ddH_2O$ treated control samples of at least three experimental repeats done in triplicate, with the standard error of mean (SEM) indicated by the error bars. $^{**}p \leq 0.01$; $^{****}p \leq 0.0001$ indicates a significant difference when compared to the control.

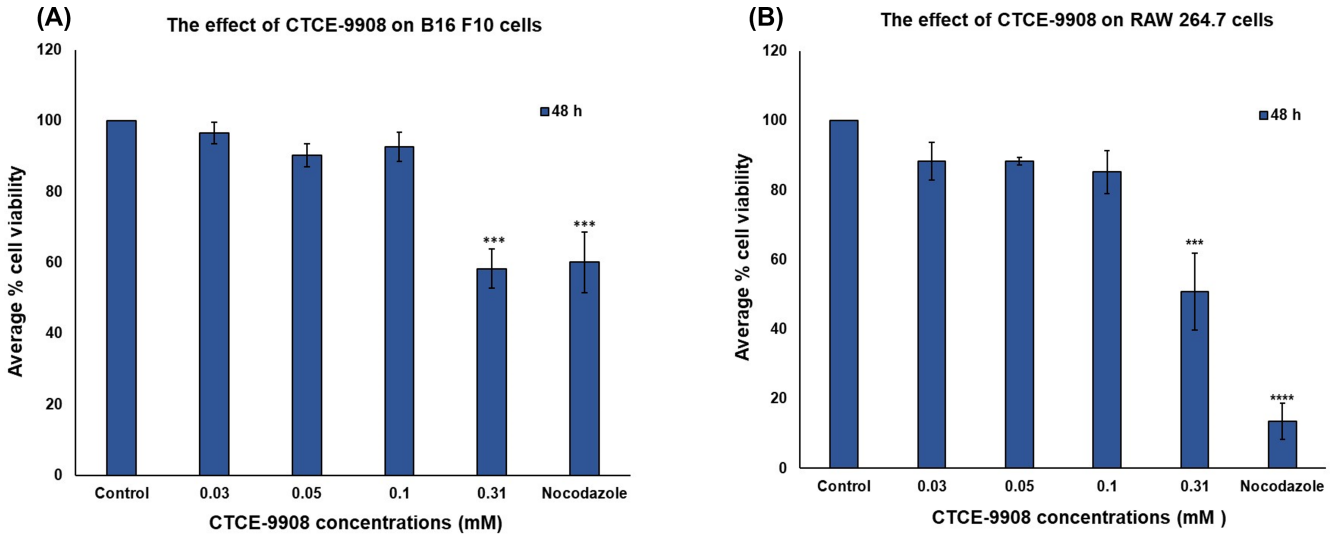


**FIGURE 2** The effect of CTCE-9908 at increased concentrations on cell viability of (A) B16 F10 and (B) RAW 264.7 cells at 48 h in vitro. Cell viability values are expressed as the percentage of viable cells relative to CCM: dd$H_2O$-treated control samples of at least three experimental repeats done in triplicate, with the standard error of the mean (SEM) indicated by the error bars. $^{**}p \leq 0.01$; $^{***}p \leq 0.001$; $^{****}p \leq 0.0001$ indicates a significant difference when compared to the control.

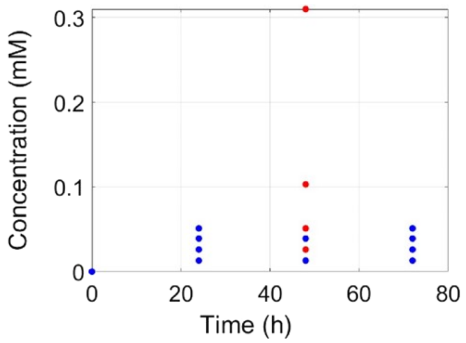


**FIGURE 3** The CTCE-9908 concentrations tested at 24, 48 and 72 h, where the blue dots represent the time points where CTCE-9908 was tested at lower concentrations and the red dots represent the time points where CTCE-9908 was tested at higher concentrations.

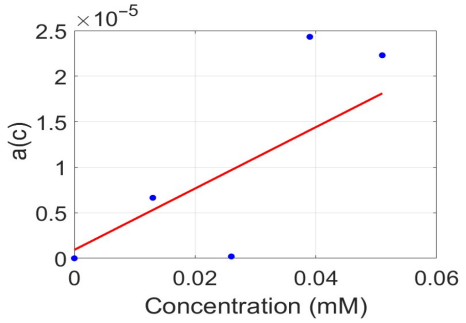


**FIGURE 4** Graphs of the values of $D$ for $c = 0, 0.013, 0.026, 0.039,$ and $0.051$ (blue dots) and the interpolating function for $c \in [0,4]$ (solid red line).

higher concentrations (at 48 h) are shown in Figure 3. The figure shows that the data is not evenly distributed in that larger concentration values occur at 48 h (indicated by the red dots). Therefore, a mathematical model was constructed to make a reasonable prediction of the cell viability having data at only a single time point, namely 48 h (Figure 3).

## 2.3 | Derivation of the cell viability function using higher CTCE-9908 concentrations

A graph of the data points and the regression function $a(c)$ for $c \in [0, 0.06]$ computed via the MATLAB software (2022b) is shown in Figure 4. The graph of $a(c)$ provides the best linear fit of the data.

Therefore, it is reasonable to consider the cell viability function, $\Psi(t)$ as

$$\Psi(t) = Ae^{-act^2}, \tag{1}$$

where the parameter $A$ compensates for potential variations in the initial states of melanoma populations, and $t$ represents time at 48 h. It is shown via the numerical computations that with the expression for $a$ in Equation (1), the cell viability function not only provides the best fit but is also consistent with the trend observed in the experiments.

## 2.4 | Estimating the parameters $A$ and $a$ for the model

The confidence bounds for parameters $A$ and $a$ were calculated with the least squares method and are displayed in Table 1, demonstrating

**TABLE 1** The parameters *A* and *a* and their corresponding 95% confidence interval.

| Cell line | A | CI | a | CI | $R_2$ |
|---|---|---|---|---|---|
| B16 F10 | 1.0190 | (0.9476, 1.0890) | $7.2690 \times 10^{-4}$ | $(4.7200 \times 10^{-4}, 9.8180 \times 10^{-4})$ | 0.8249 |
| RAW 264.7 | 0.9108 | (0.839, 0.9826) | $4.906 \times 10^{-4}$ | $(2.288 \times 10^{-4}, 7.523 \times 10^{-4})$ | 0.6459 |

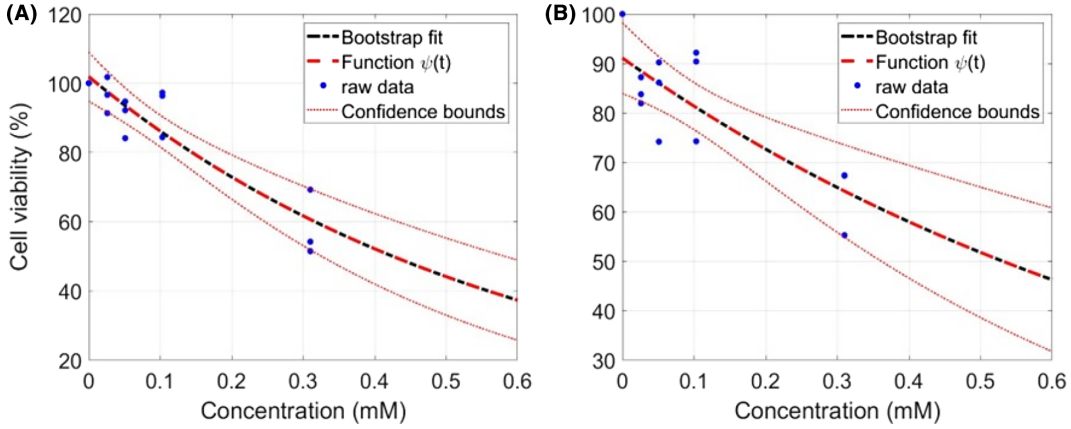


**FIGURE 5** A two-dimensional representation of the cell viability versus concentration of CTCE-9908 in (A) B16 F10 and (B) RAW 264.7 cells. The dashed line in red represents the best fit generated by (1) using the nonlinear least squares, the dashed-dotted line in black demonstrates the best fit generated by (2) using the bootstrap method, the dotted lines in red represent the 95% confidence interval computed by the nonlinear least squares and the blue dots portray the raw data.

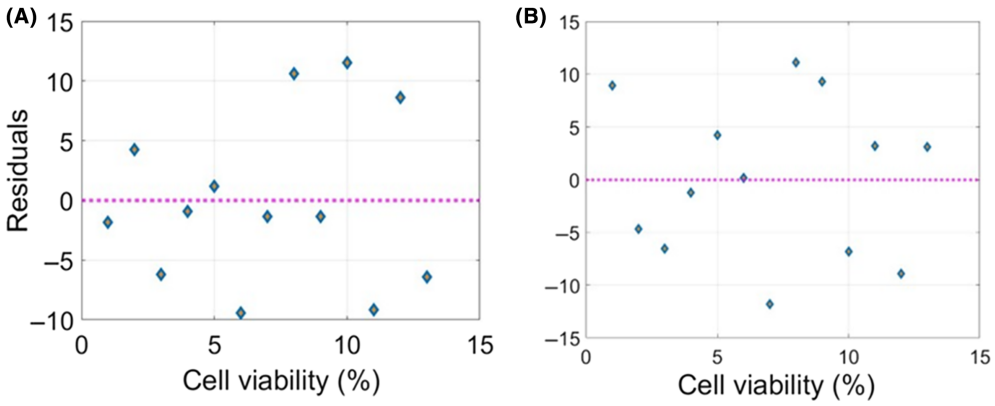


**FIGURE 6** Distribution of residuals corresponding to various concentrations in (A) B16 F10 and (B) RAW 264.7 cells. The blue diamonds represent the residuals, and the dotted lines depict a zero line. Because the residuals are randomly distributed around the zero line, it indicates that the model fits the data properly.

that all the parameters are within the bounds of the confidence interval. This means the model fits the data well and the parameters are stable. The higher value of $R^2$ can further confirm this.

Figure 5 shows the graphical presentation of the numerical output of the fitting process generated by Model 2 via the nonlinear least squares and the bootstrap method. The dashed-dotted line in black represents the bootstrap fit; the dashed line in red depicts the fit via the nonlinear least squares; the red dotted lines represent the 95% confidence bounds; and the blue dots show the raw data. The graphs generated by the nonlinear least squares and bootstrap methods are visually indistinguishable. Both graphs fall within the 95% confidence interval.

The behaviour of the residuals corresponding to various concentrations is given in Figure 6, where the residuals are randomly scattered around the zero line. This further supports the theoretical results about how the model provides a good data description. Furthermore, the bootstrap distributions of parameters *A* and *a* are within their associated confidence bounds.

A graphical representation of the distribution of the parameters and their confidence bounds is provided in Figure 7, where the vertical dotted lines in red represent the 95% confidence interval, and the histograms represent the distribution of the coefficients.

## 2.5 | Determining the IC50 of CTCE-9908

The cell viability model is presented in Anguelov et al.[11] 1 as a function of both concentration and time. The significance of presenting the function in this manner is that one determines the cell viability

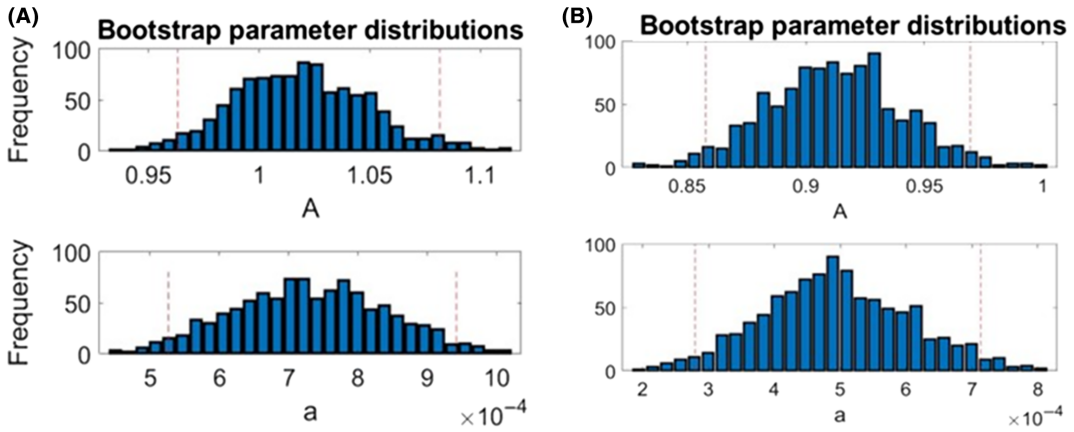


**FIGURE 7** The bootstrapped distribution of the parameters *A* and *a* and their respective confidence intervals in (A) B16 F10 and (B) RAW 264.7 cells. The vertical red dotted lines represent the 95% confidence bounds.

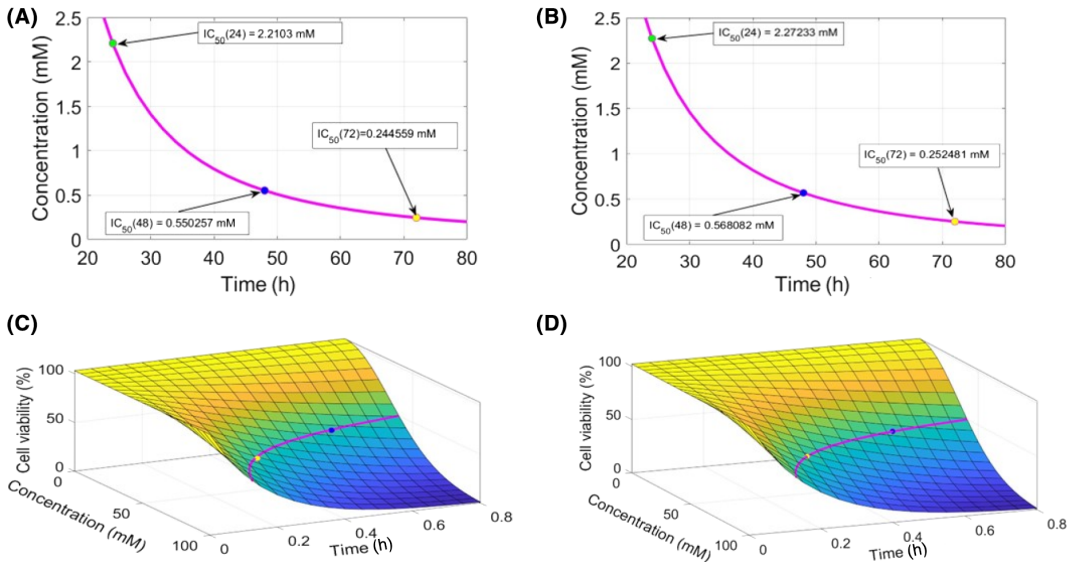


**FIGURE 8** The $IC_{50}$ curve as a function of time of CTCE-9908 in (A) B16 F10 cells and (B) RAW 264.7 cells. A three-dimensional graph of the cell viability as a function of time and concentration as defined in Equation (2) in (C) B16 F10 cells and (D) RAW 264.7 cells. A green dot represents the $IC_{50}$ at 24 h, a blue dot shows the $IC_{50}$ at 48 h, and a yellow dot represents the $IC_{50}$ at 72 h.

and concentration at any given time. Thus, Anguelov et al.[11] 1 becomes

$$\Psi(c,t) = Ae^{-ac(c)t^2}, \text{for } c \in [0,0.8], t \in 0,100 \quad (2)$$

The corresponding graph of the three-dimensional representation of Equation (2) and the $IC_{50}(t)$ function is provided in Figure 8 with $c \in [0,0.8]$ and $t \in [0,72]$. This function represents the concentration and time values required to reduce the population by half. Thus, it enables one to read the values of both time and concentration, which reduces the population by half. To demonstrate this, one can observe from the figure that the $IC_{50}$ at 24 h in B16 F10 cells is 2.2103 mM; the $IC_{50}$ at 24 h in RAW 264.7 cells is 2.63862 mM; the $IC_{50}$ at 48 h in B16 F10 cells is 0.550257 mM; the $IC_{50}$ at 48 h in RAW 264.7 cells is 0.659656 mM; the $IC_{50}$ at 72 h in B16 F10 cells is 0.244559 mM; the $IC_{50}$ at 72 h in RAW 264.7 cells is 0.293180 mM. A two-dimensional and three-dimensional display of the $IC_{50}(t)$ is given in Figure 8, which shows the $IC_{50}(t)$ plotted on the surface. As noted earlier, this curve represents the intersection with the horizontal plane, which corresponds to 50% of cell viability.

The model provided in Equation (2) and the numerical simulations presented here clearly show that the cell viability data obtained at $t = 48$ h can accurately be forecasted to other timelines; that is, $t = {}_{[0,100]}$ h.

## 2.6 | Area under the curve

The area under the curve (AUC) is a well-known robust metric to compare the potency of a drug across cell lines and to indicate cell line

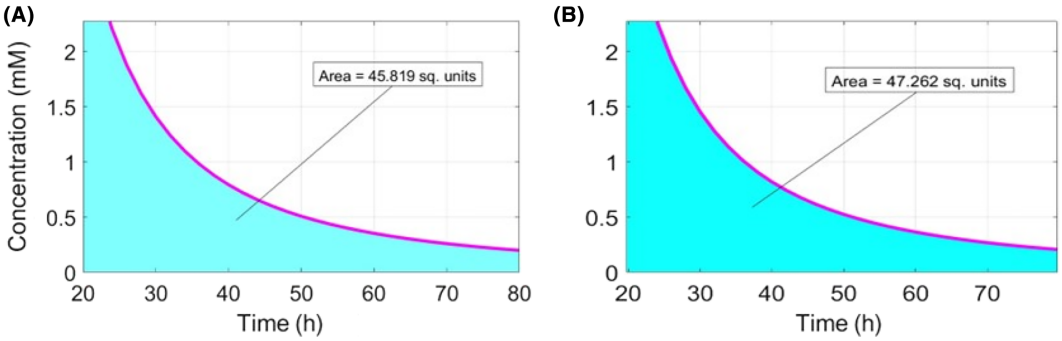


**FIGURE 9** The area under the curve as a function of time of CTCE-9908 in (A) B16 F10 cells and (B) RAW 264.7 cells.

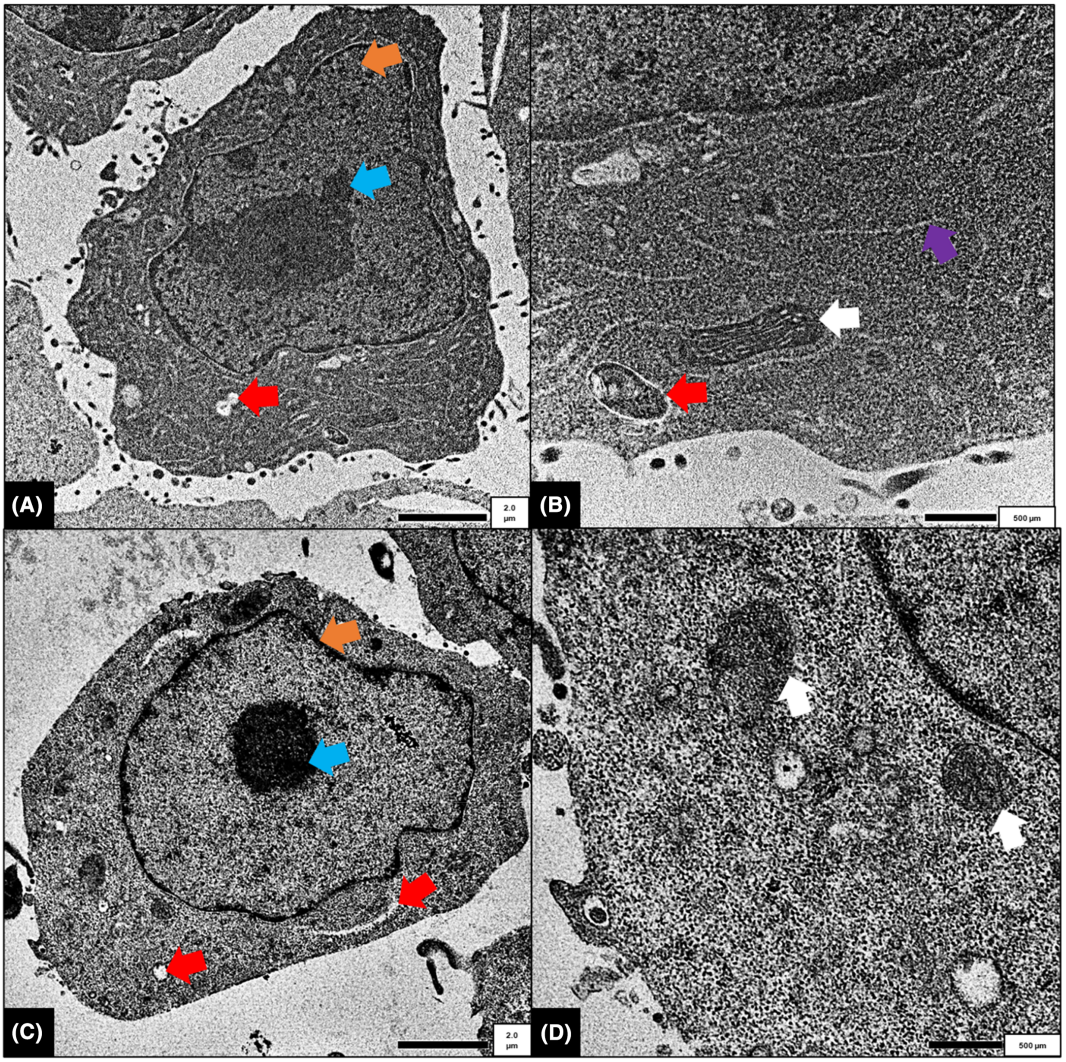


**FIGURE 10** Transmission electron micrographs of $ddH_2O$-treated B16 F10 (A, B) and RAW 264.7 (C, D) cells at 48 h. The scale bar at the bottom right corner represents 2 μm (A, C) at 3000× magnification and 500 μm (B, D) at 10 000× magnification. Red arrows indicate lysosomes and vacuoles; white arrows indicate mitochondria; orange arrows indicate the nucleus; light blue arrows indicate the nucleolus, and purple arrows indicate rough endoplasmic reticulum.

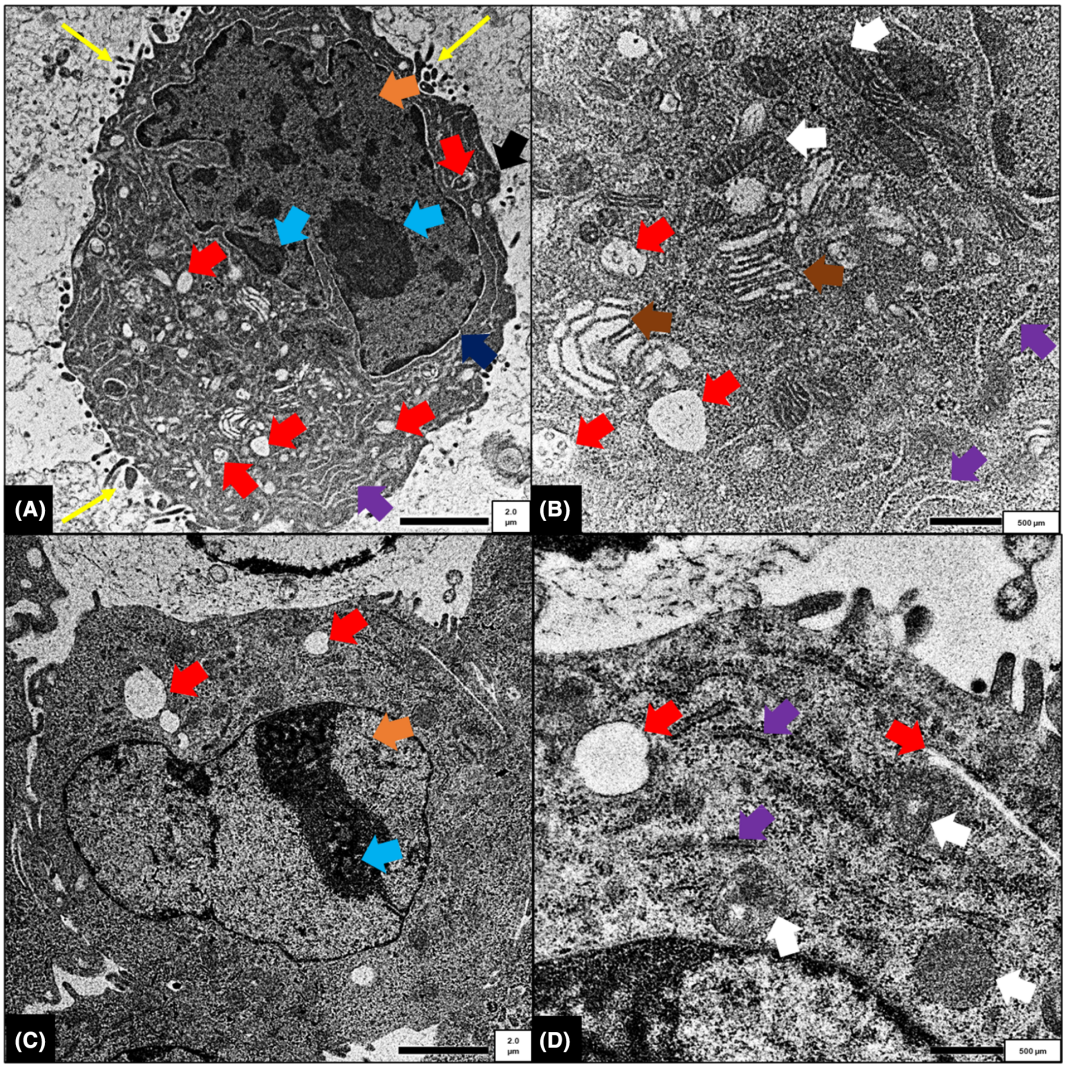


**FIGURE 11** Transmission electron micrographs of CTCE-9908-treated B16 F10 (A, B) and RAW 264.7 (C, D) cells at 0.53 mM after 48 h. The scale bar represents 2 µm (A, C) at 3000× magnification and 500 µm (B, D) at 10 000× magnification. Red arrows indicate lysosomes and vacuoles; white arrows indicate mitochondria; orange arrows indicate nucleus; light blue arrows indicate nucleolus; purple arrows indicate rough endoplasmic reticulum; yellow arrows indicate apoptotic bodies; brown arrows indicate Golgi complex; dark blue arrows indicate slight swelling of the perinuclear space and black arrows indicate membrane blebbing.

selectivity.[13] As such, CTCE-9908 demonstrated a slightly lower AUC for B16 F10 cells (45.819 square units) compared to RAW 264.7 cells (47.262 square units) (Figure 9).

## 2.7 | Transmission electron microscopy

The $ddH_2O$-treated B16 F10 control cells (Figure 10A,B) displayed clearly defined nuclei and nucleoli. Even though some lysosomes and vacuoles were present (red arrows), the mitochondria and the rough endoplasmic reticulum (RER) remained unaffected. The $ddH_2O$-treated RAW 264.7 control cells (Figure 10C,D) displayed clearly defined nuclei and nucleoli. Although some lysosomes and vacuoles were present, the mitochondria remained unaffected.

CTCE-9908-treated B16 F10 cells (Figure 11A,B) displayed morphological changes such as the crenated profile of the nuclear membrane, initial stages of nuclear margination, membrane blebbing, apoptotic bodies and the swelling of the Golgi apparatus. An increased amount of lysosomes and vacuoles was present, with slight swelling of the rough endoplasmic reticulum (RER), indicating endoplasmic reticulum stress. Furthermore, CTCE-9908 induced slight swelling of the perinuclear space while mitochondria remained unaffected. The CTCE-9908-treated RAW 264.7 cells (Figure 11C,D) displayed clearly defined nuclei and nucleoli, with initial stages of nuclear margination. Although some lysosomes and vacuoles were present, the mitochondria and the RER remained unaffected.

Nocodazole-treated B16 F10 cells (Figure 12A,B) displayed morphological changes, including the formation of myelin figures and an

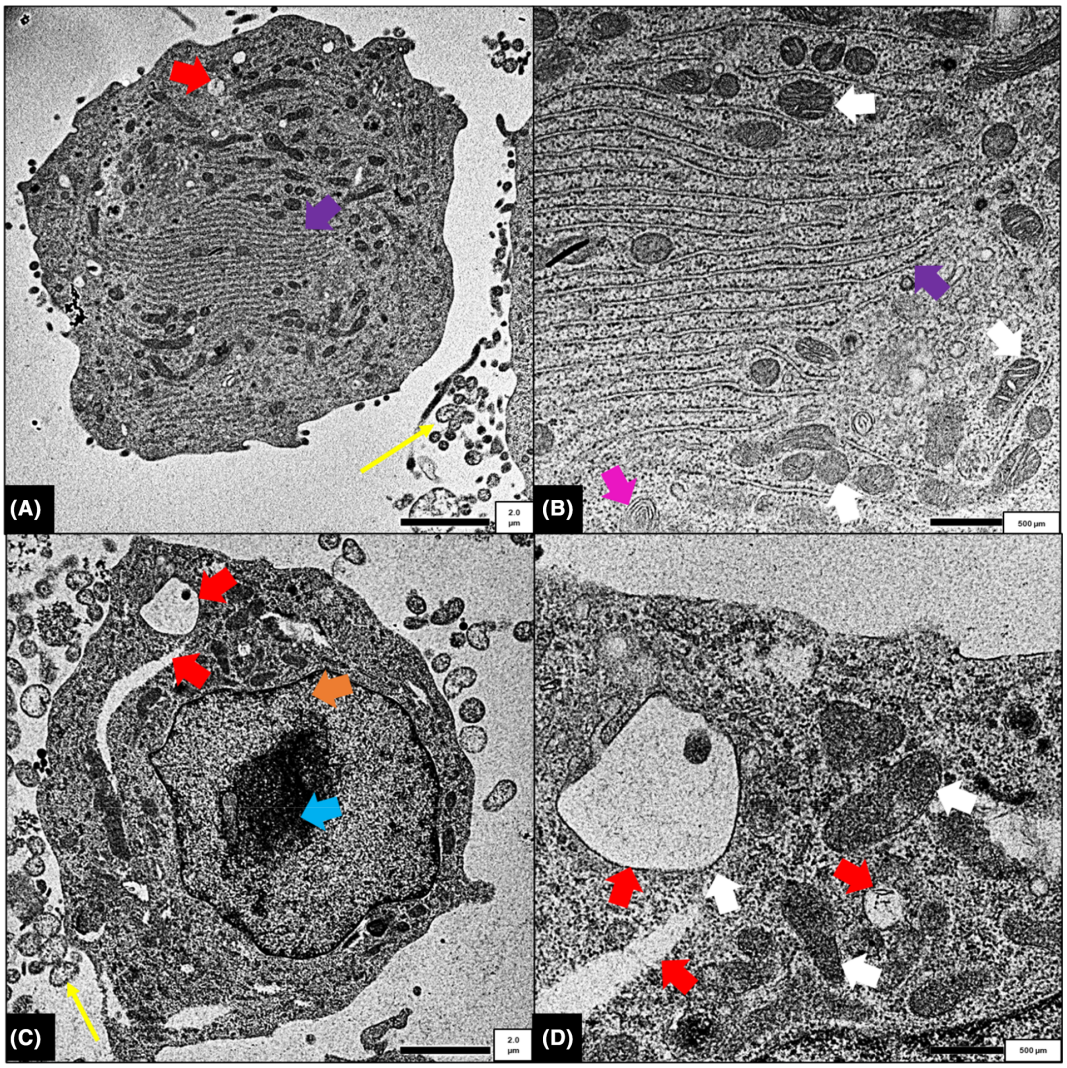


**FIGURE 12** Transmission electron micrographs of nocodazole-treated B16 F10 (A, B) and RAW 264.7 (C, D) cells at 1.30 mM after 48 h. The scale bar represents 2 µm (A, C) at 3000× magnification and 500 µm (B, D) at 10 000× magnification. Red arrows indicate lysosomes and vacuoles; white arrows indicate mitochondria; purple arrows indicate rough endoplasmic reticulum; yellow arrows indicate apoptotic bodies; pink arrows indicate myelin figures; orange arrows indicate the nucleus and light blue arrows indicate the nucleolus.

increased amount of RER as well as lysosomes and vacuoles, while mitochondria remained unaffected. Nocodazole-treated RAW 264.7 cells (Figure 12C,D) displayed apoptotic body formation and increased lysosomes and vacuoles, while mitochondria remained unaffected.

## 2.8 | Cell cycle progression

CTCE-9908 exposure at 0.05 mM did not induce statistically significant results in either cell line compared to the $ddH_2O$-treated control cells. In addition, both NOC-treated B16 F10 and RAW 264.7 cells induced a reduction in the G1 cell populations (23.13 ± 2.94 for B16 F10 cells and 17.21 ± 6.22 for RAW 264.7 cells) compared to $ddH_2O$-treated cells (73.74 ± 1.81 for B16 F10 cells and 72.74 ± 8.14 for RAW 264.7 cells). In addition, NOC-treated B16 F10 and RAW 264.7 cells induced an increase in the G2/M cell populations (43.01 ± 3.16 for B16 F10 cells and 50.04 ± 11.93 for RAW 264.7 cells) (Figure 13) compared to $ddH_2O$-treated cells (15.31 ± 1.81 for B16 F10 cells and 7.17 ± 1.33 for RAW 264.7 cells).

## 2.9 | Caspase-3 activation

Neither CTCE-9908 nor NOC induced significant caspase-3 in either the B16 F10 or RAW 264.7 cell line when compared to the control cells treated with $ddH_2O$ (Figure 14A). Actinomycin D, an apoptotic inducer, was used as a positive control and induced statistically significant effects in B16 F10 ($p < 0.0001$) and RAW 264.7 ($p < 0.0001$) cells.

## 2.10 | ERK1/2 activation

Both CTCE-9908 (63.59 ± 3.00) ($p = 0.0133$) and nocodazole (78.91 ± 1.71) ($p = 0.0038$) exposure significantly inhibited ERK1/2

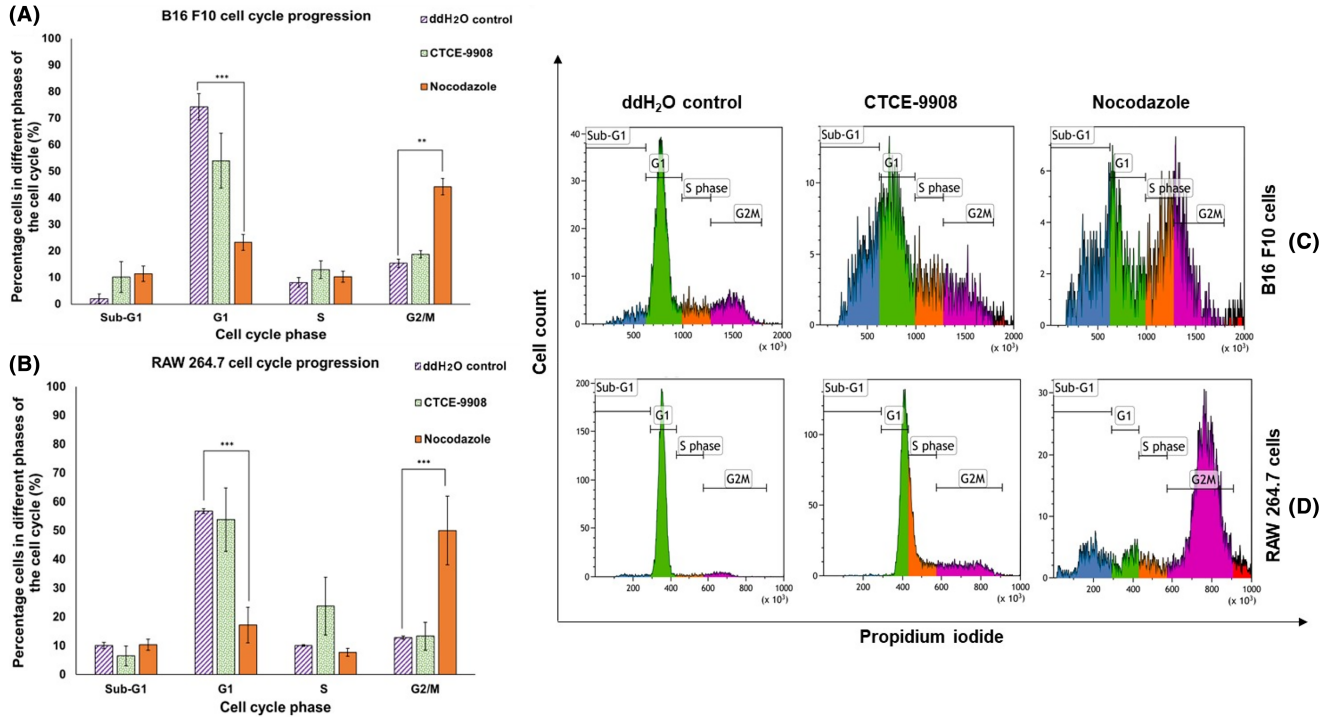


**FIGURE 13** Quantitative representation of the percentage (A) B16 F10 cells and (B) RAW 264.7 cells in the different phases of the cell cycle (sub-G1, G1, S and G2/M) after 48 h of exposure to $ddH_2O$, CTCE-9908 at 0.05 mM and NOC at 1.30 mM and flow cytometry histograms for cell cycle analysis in (C) B16 F10 cells and (D) RAW 264.7 cells. The bar graphs represent the average of four experimental repeats, with the standard error of mean (SEM) indicated by the error bars. $^{**}p \leq 0.01$; $^{***}p \leq 0.001$ indicates significant difference when compared to the control treated with $ddH_2O$.

activation in the B16 F10 cell line, compared to the control cells treated with $ddH_2O$ (93.75 ± 0.74) (Figure 14B). However, neither ERK1/2 overactivation nor a significant difference between the control and compound-treated cells was observed in the RAW 264.7 cell line.

## 2.11 | CXCR4 activation

Neither CTCE-9908 nor NOC induced significant changes in CXCR4 activation in either the B16 F10 or RAW 264.7 cell line when compared to the control cells treated with $ddH_2O$ (Figure 14C).

## 2.12 | CXCL12 expression

Neither CTCE-9908 nor NOC induced significant changes in CXCL12 expression in either the B16 F10 or RAW 264.7 cell line when compared to the control cells treated with $ddH_2O$ (Figure 14D).

# 3 | DISCUSSION

The activation of the CXCR4/CXCL12 axis is known to activate downstream signalling pathways in cancer cells to regulate cell processes such as proliferation and cell survival.[14] A recent review article concluded that CTCE-9908 (a CXCR4 inhibitor) might inhibit these downstream signalling pathways of the CXCR4/CXCL12 axis in melanoma cells by competitively binding to CXCR4.[1] In vitro evidence suggests that pre-treatment with CTCE-9908 previously inhibited proliferation, adhesion, migration and invasion in osteosarcoma cells.[12] Other in vitro studies found that CXCR4 antagonists, such as AMD3100 and TC140012, inhibited the proliferation of cancer cells, such as undifferentiated thyroid cancer and acute lymphoblastic leukaemia cells.[15,16] Therefore, the cytotoxicity and cell death mechanisms of CTCE-9908 towards CXCR4-expressing cell lines, namely B16 F10 (a metastatic melanoma cell line) and RAW 264.7 (a non-cancerous macrophage cell line), were investigated in this study.

In this study, cytotoxicity through crystal violet staining revealed that CTCE-9908 did not induce statistically significant cytotoxic effects at lower concentrations ranging from 0 to 0.051 mM. The CTCE-9908 concentrations were therefore increased (0–0.31 mM), and statistically significant cytotoxic effects were obtained for both cell lines at 0.31 mM after 48 h. These findings are supported by Wong,[17] who indicated that CTCE-9908 at lower concentrations (10 ng/mL–100 μg/mL) did not induce cytotoxic effects in a prostate cancer cell line.[17] In the current study, mathematical modelling allows for the approximation of parameters outside the current dataset and the prediction of data for the increased CTCE-9908 concentrations. Furthermore, the mathematical model enabled the prediction of $IC_{50}$

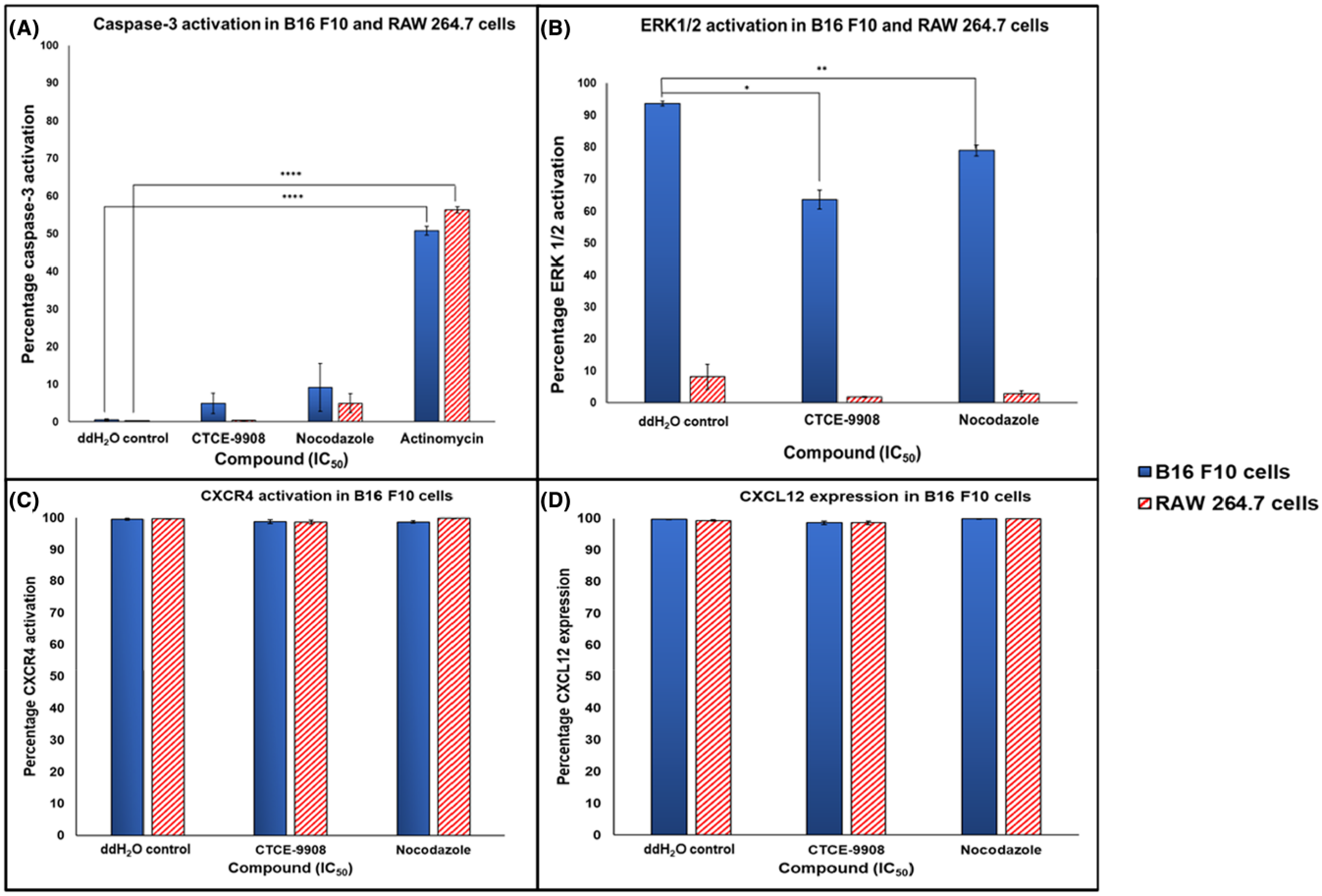


**FIGURE 14** Quantitative representation of the percentage (A) caspase-3 activation, (B) ERK1/2 activation, (C) CXCR4 activation and (D) CXCL12 expression in B16 F10 cells and RAW 264.7 cells after 48 h after exposure to $ddH_2O$, CTCE-9908 at 0.05 mM, NOC at 1.30 mM and actinomycin D at 0.01 Um. The bar graphs represent the average of four experimental repeats, with the standard error of the mean (SEM) indicated by the error bars. $^*p \leq 0.05$; $^{**}p \leq 0.01$; $^{****}p \leq 0.0001$ indicates significant difference when compared to the control treated with $ddH_2O$.

at any time point in a range from 0 to 100 h. As a result, mathematical modelling found no significant difference between the $IC_{50}$ or AUC between the B16 F10 and RAW 264.7 cell line, suggesting non-selective cytotoxicity of CTCE-9908 towards melanoma cells. This might be explained by the fact that CXCR4 is expressed in various cell lines, including melanoma[18] and RAW 264.7 cells.[19] The authors, therefore, suggest that these results should be confirmed in other melanoma and non-cancerous cell lines.

This current study used TEM to observe intracellular morphological changes induced by CTCE-9908 at $IC_{50}$ on B16 F10 and RAW 264.7 cells. As seen in CTCE-9908-treated B16 F10 cells, an increased amount of lysosomes and vacuoles is indicative of cell death.[20] Kwong et al. previously demonstrated that CTCE-9908 induced cell death in ovarian cancer cells and that cell death correlated with CXCR4 expression, as CTCE-9908 induced significant morphologic changes in CXCR4-expressing ovarian cancer cells but not in CXCR4 negative cell lines.[21] In support of these findings, a previous study found that another CXCR4 antagonist (AMD3100) induced morphological changes, such as an increase in the amount of cytoplasmic vacuoles after 9 days of exposure to U937 cells.[22] Moreover, morphological changes seen in B16 F10 melanoma cells, such as the crenated profile of the nuclear membrane, initial stages of nuclear margination, membrane blebbing, apoptotic bodies and the swelling of the Golgi apparatus, are all ultrastructural morphological characteristics of apoptotic cells.[23] In addition, initial stages of nuclear margination were also observed in the RAW 264.7 cells treated with CTCE-9908. The current study demonstrates that CTCE-9908 induced slight swelling of the perinuclear space in B16 F10 cells. Shaiken et al. previously suggested that the perinuclear space might be the site for signal transduction, where oncogenic proteins such as Ras, Src or p53 are retained. For this reason, they proposed that the perinucleus might play a genomic-protective role in cancer.[24] In addition, another study found that a swollen perinucleus was prevalent in hypoxic A549 cells and was described as a sign of autosis, a sub-type of autophagy.[25] Additionally, endoplasmic reticulum stress, as observed in CTCE-9908-treated cells, might indicate the activation of autophagic pathways, which might lead to cell death. However, cell fate depends on the intensity and duration thereof.[26]

Furthermore, it is well known that the activation of the CXCR4/CXCL12 axis activates the ERK1/2 MAP-K cascade,[27] which

promotes cell proliferation, differentiation and survival.[28] Marampon et al. previously described a correlation between ERK1/2 and tumour growth, which led the authors to explore the effects on ERK1/2 in response to CTCE-9908-treatment in B16 F10 melanoma and RAW 264.7 cells. However, the authors were interested in investigating cell survival at a non-cytotoxic concentration (10 times lower than the $IC_{50}$), where the RAW 264.7 cells remain unaffected. The results indicate that CTCE-9908 at a non-cytotoxic concentration of 0.05 mM significantly inhibited ERK1/2 in B16 F10 cells but not in RAW 264.7 cells, as ERK1/2 expression was low in this non-cancerous cell line. A previous study also found that ERK1/2 inhibition was observed in response to blocking the CXCR4/CXCL12 axis with inhibitors, such as LY2624587 and AMD3100.[29]

Interestingly, the current study did not observe changes in CXCR4 activation and CXCL12 expression at the concentration 10 times lower than the $IC_{50}$, suggesting that ERK1/2 inhibition does not exclusively occur downstream of CXCR4 inhibition, as previously suggested.[1] Furthermore, the inhibition of ERK1/2 by CTCE-9908 might indicate its potential anti-metastatic properties, as ERK1/2 is also associated with tumour metastasis.[30] These findings reveal that CTCE-9908 might demonstrate anti-metastatic effects, such as the inhibition of cell survival independent of cytotoxicity.

Based on the fact that CTCE-9908 inhibits cell survival pathways at a lower concentration (10 times lower than the $IC_{50}$), cleaved caspase-3 levels were also investigated at 0.05 mM to explore the possibility of apoptotic cell death in CTCE-9908-treated B16 F10 and RAW 264.7 cells, as cleaved caspase-3 is a known apoptotic marker.[31] However, CTCE-9908 did not increase caspase-3 as a measure of apoptosis in this study. In support of these findings, a previous study by Kwong et al. concluded that CTCE-9908 (at 300 μg/mL) did not induce apoptosis or cellular senescence but induced cell death by mitotic catastrophe, as characterised by large, multi-nucleated ovarian cancer cells.[21] To substantiate the notion that CTCE-9908 might induce non-apoptotic types of cell death in B16 F10 melanoma cells, the cell cycle distribution after treatment of CTCE-9908 at 0.05 mM was investigated. A previous study found that treatment with another CXCR4 inhibitor (AMD3100) at 0–30 mM for 7 days in acute myeloblastic leukaemia cells induced features of apoptosis, indicated by an increased number of cells in the sub-G1 phase of the cell cycle.[22] However, the current study found that CTCE-9908 at 0.05 mM (10 times lower than the $IC_{50}$) did not induce changes in cell cycle distribution. Similar to these results, a previous study demonstrated that a CXCR4 antagonist (AMD3100) at 10 μM for 72 hours did not induce significant cell cycle alterations in Ewing sarcoma cell lines in vitro.[32] In contrast, CTCE-9908-treated ovarian cancer cells at 100 and 300 μg/mL previously led to G2/M arrest in a concentration and time-dependent manner. Importantly, CXCR4-negative cells did not undergo G/M arrest in response to CTCE-9908 treatment.[21] These considerations led the authors to suggest that each CXCR4 inhibitor might exert a different mechanism of action that is cell-line dependent and that future studies should be aimed at investigating these effects on other melanoma and non-cancerous cell lines.

Overall, this study developed a mathematical model for CTCE-9908-treatment in B16 F10 and RAW 264.7 cells, which contributes to the knowledge of CTCE-9908 cytotoxicity and demonstrates that the compound inhibits cell proliferation at the calculated $IC_{50}$. Furthermore, this study demonstrated that CTCE-9908 induced ultrastructural morphological changes in B16 F10 and RAW 264.7 cells at $IC_{50}$ concentration. However, apoptotic cell death was not induced by CTCE-9908 at a concentration 10 times lower than the $IC_{50}$, as determined by non-significant differences in caspase-3 and cell cycle distribution. Interestingly, a non-cytotoxic concentration of CTCE-9908 led to cell survival inhibition (measured by ERK1/2) in B16 F10 melanoma cells and not in non-cancer cells (RAW 264.7 cells) but not through downstream signalling of CXCR4. These results also suggest that CTCE-9908 might demonstrate other anti-metastatic effects, such as the inhibition of cell survival independent of cytotoxicity or CXCR4 inhibition. However, the authors recommend that future research on other melanoma and non-cancerous cell lines is necessary to substantiate the findings of this study and provide in-depth mechanistic insights on CTCE-9908-induced cell death against melanoma cells.

## 4 | METHODS

### 4.1 | Cell lines

This section discusses the melanoma (B16 F10) and the macrophage (RAW 264.7) cell lines that were used in this study.

#### 4.1.1 | Melanoma

The melanoma (B16 F10) cell line is a melanin-producing metastatic cell line isolated from the skin tissue of a mouse with melanoma and is often used for melanoma research.[33] The B16 F10 cell line was purchased from the American Type Culture Collection B16 F10 (ATCC CRL-6475) and used between passages 4 and 12.

#### 4.1.2 | Non-metastatic monocyte/macrophage cells

The RAW 264.7 cell line was used as the control cell line. RAW 264.7 is a non-cancerous, monocyte/macrophage-like cell line[34] and was chosen as it also expresses CXCR4.[19] This cell line was purchased from CELLONEX, South Africa and used between passages 6 and 20.

### 4.2 | Sample preparation

The controls for both cell lines (used to determine the effects of CTCE-9908) were cells exposed to the complete culture medium (CCM): double distilled ($ddH_2O$) in a 1:1 ratio. The current study examined the effects of CTCE-9908 on melanoma, with an emphasis on selective cytotoxicity on melanoma. Therefore, all the outcomes were compared to a non-selective cytotoxic drug, such as nocodazole (NOC), to effectively illustrate the ability of CTCE-9908 to serve as

targeted therapy towards melanoma.[35] The positive controls were cells exposed to 1.30 mM NOC, which is a microtubule disruptor. NOC was dissolved in dimethyl sulfoxide (DMSO) and diluted with $ddH_2O$, ensuring final DMSO concentrations of <0.01% v/v. CTCE-9908 and NOC were purchased in powder form. CTCE-9908 was reconstituted in double distilled water ($ddH_2O$). Actinomycin D (an apoptotic inducer)[36] was used as a positive control for caspase-3 assays at 0.01 uM in $ddH_2O$. Stock solutions of each of the compounds were aliquoted and stored at −20°C to maintain integrity. Prior to each experiment, the compounds were thawed and thoroughly mixed, thereby ensuring consistency throughout experiments.

## 4.3 | General cell culture maintenance

The cells were cultured and maintained following the procedures outlined in the study by Basson et al. Briefly, the cells were cultured in sterile culture flasks in a culture medium called CCM, which consisted of Dulbecco's modified essential medium (DMEM), 10% fetal calf serum (FCS) and 1% antibiotics (amphotericin/penicillin/streptomycin). This culture was maintained in a humidified atmosphere at 37°C with 5% $CO_2$ using a Forma Scientific water-jacketed incubator. B16 F10 cells were detached using TrypLE Express phenol red, while RAW 264.7 cells were detached using a method previously described.[35]

## 4.4 | Crystal violet staining

Crystal violet staining was performed. In summary, B16 F10 melanoma cells were seeded at a cell density of 5000 cells per well and RAW 264.7 cells at 10 000 cells per well in 96-well plates. Cells were incubated for 24 h in a humidified incubator at 37°C with 5% $CO_2$ to allow cell attachment. Cells were exposed to CTCE-9908 (0–0.051 mM) for 24, 48 and 72 h. Increased CTCE-9908 concentrations (0.1 and 0.31 mM) were tested on cells at 48 hours. NOC was used as a positive control at 1.30 mM. After exposure, the cells were fixed with 1% glutaraldehyde and incubated for 30 min to terminate each experiment.

Crystal violet at 0.1% was used to stain the cells at room temperature for 30 min. Tap water was used to rinse the plates, leaving them to dry. Crystal violet was solubilised with 100 µL of 10% acetic acid, and the absorbance was measured at a wavelength of 570 nm. Results show the percentage cell viability in relation to the control (CCM: $ddH_2O$), and the $IC_{50}$ values were calculated using GraphPad Prism v6.01 (California, USA). The B16 F10 CTCE-9908 $IC_{50}$ at 48 h was tested with the crystal violet assay in vitro to compare the calculated $IC_{50}$ to its actual effect on both cell lines.

## 4.5 | Mathematical modelling of CTCE-9908 inhibition using nonuniformly distributed data

Due to CTCE-9908 being a costly compound, a full range of serial dilutions at three timelines (24, 48 and 72 h) was not possible. Therefore, a mathematical model was constructed to predict the cell viability at higher CTCE-9908 concentrations from 0 to 100 h, using the data obtained for increased CTCE-9908 concentrations at 48 h. The accuracy of predictions produced via interpolation, linear or nonlinear regression at any given value of an independent variable depends on the density of data points around this value. Extrapolation (predictions outside the domain) significantly depends on the type of functions used in the fitting process and, to a lesser extent, on the accuracy of the approximations of the data. Therefore, the mathematical modelling process is focused on appropriately deriving a type of function to be used in the approximation/fitting process, which consists of the following steps:

i. A mathematical model of the processes tested in the experiment is constructed based on known quantitative relationships.
ii. The measured or observed variable is derived from the model in terms of its parameters.
iii. The form of the theoretically derived observable determines the type of function to be fitted to the data. This is a function of the independent variable, which depends on a certain number of parameters.
iv. The function in (iii) is fitted to the data to identify the values of the parameters.

The advantage of this approach is that the domain of validity of the approximation is determined by the domain of validity of the model and not the location of the data. Furthermore, the $IC_{50}$ is presented as a function of time. The practical value of the latter is that one can obtain cell viability at a specific concentration and at a given time.

The parameter $a$ captures the response to a change in the concentration of the inhibitor. Hence, the parameter $a$ is a function of concentration, $c$, which is denoted as $a(c)$. A cell viability function is an extension of the cell viability function derived from.[11] It was determined how parameter $a$ relates to the concentration $c$, and the function $a(c)$ was derived that provides the best linear fit for the data. To do so, the function $a(c)$ was approximated via linear regression initiated at the origin. The parameters were computed with the function ψ(t) using the MATLAB (2022b) *fminsearch* function. The mathematical model was validated using (i) nonlinear least squares and (ii) the bootstrapping method to examine the stability of the estimated coefficients.

## 4.6 | Transmission electron microscopy

B16 F10 and RAW 264.7 cells were seeded in T25 $cm^2$ tissue culture flasks at a concentration of $20 \times 10^4$ cells per mL in 4.5 mL ($9 \times 10^5$ cells in the flask). Cells were treated with the B16 F10 CTCE-9908 $IC_{50}$ at 48 h and a CCM:$ddH_2O$ as well as a NOC-treated positive control were included. Cells were harvested and collected after 48 h, and cells were washed with 0.1 M PBS. Every wash included a 504 x *g* centrifugation step. Following an hour-long fixation with a 2.5% glutaraldehyde/formaldehyde solution, the cells were washed three times with 0.1 M PBS for a total of 10 min. The

cells were suspended in 1 mL of osmium tetroxide solution (1% for 1 h), washed three times with 0.1 M PBS for 10 min, and dehydrated with 30%, 50%, 70% and 90%, and three times with 100% ethanol (10 min each). Propylene oxide was added to the cell pellet (10 min). The cell pellet was then suspended in a 2:1 combination of propylene oxide and epoxy resin (1 h) and placed on an inclined rotator. After an hour, the cell pellet was suspended in a 1:2 combination of propylene oxide and epoxy resin and kept on an inclined rotator overnight. The pellet was then transferred to a microcentrifuge tube and set in 100% epoxy resin in an oven (65°C for 36 h). Using a microtome, the moulds were then cut into ultra-thin sections with glass and then a diamond knife. After being stained with urinyl acetate for 5 min, the samples were then rinsed three times in $ddH_2O$. After being stained with lead citrate for 2 min, the samples were then rinsed three times in $ddH_2O$. Samples were blotted and dried before viewing them with a transmission electron microscope, JOEL JEM-2100F, 200 kV FE (Field Emission) microscope (Peabody, Massachusetts, USA).

## 4.7 | Flow cytometric analyses

B16 F10 and RAW 264.7 cells were seeded in T75 $cm^2$ tissue culture flasks at a concentration of $70 \times 10^4$ cells per mL in 9 mL ($6.3 \times 10^6$ cells in the flask). After 24 hours, the cells were treated with a reduced CTCE-9908 concentration due to non-significant differences observed between B16 F10 and RAW 264.7 cells in viability assays. Therefore, to investigate the effects of CTCE-9908 at a concentration that is not cytotoxic to RAW 264.7 cells, a CTCE-9908 concentration at 10 times lower than the $IC_{50}$ (0.05 mM) was used for flow cytometric assays. After 48 hours, cells were harvested, centrifuged at 504 x *g* for 5 min, washed twice with ice-cold PBS, fixed in ice-cold 70% methanol and stored at −20°C until further analysis. After staining and prior to analyses, the cells were vortexed and subsequently analysed on the Flow Check Pro (Beckman Coulter, Miami, USA) attached to an air-cooled argon laser. Analysed data was derived from a minimum of 15 000 cells using Kaluza C data analysis software (Version 1.1.00003.20057 Beckman Coulter). Debris and doublets were gated out and excluded from further analyses. All flow cytometry data is representative of four experimental repeats ($n = 4$), with results given as mean ± standard error of the mean (SEM).

### 4.7.1 | Cell cycle progression

Cell pellets containing $1 \times 10^6$ cells were washed with 0.5% bovine serum albumin (BSA)/PBS buffer and centrifuged at 504 x *g* for 3 min. Cell pellets were resuspended in 500 µL of 0.1 M PBS containing propidium iodide (PI) (40 µg/mL), RNase (100 µg/mL) and 0.1% Triton X-100 and incubated for 40 min at 37°C and 5% $CO_2$ in a humidified incubator in the dark.

### 4.7.2 | Protein activation of ERK1/2

After washing the samples once with 0.5% (w/v) BSA in PBS buffer, $1 \times 10^6$ cells per sample were suspended in 5 µL Phos-ERK1 (T202/Y204)/ERK2 (T185/Y187) Alexa Fluor 488-conjugated antibody from R&D systems (supplied in a saline solution containing BSA and sodium azide) at 0.95 µg/mL in sterile PBS and incubated for 40 min at 2–8°C.

### 4.7.3 | Apoptosis detection with caspase-3

After washing the samples once with 0.5% (w/v) BSA in PBS buffer, $1 \times 10^6$ cells per sample were suspended in 0.25 µg mouse cleaved anti-caspase-3 (asp 175) 405 nm from R&D Systems at 0.5 mg/mL in sterile PBS and incubated for 40 min at 2–8°C.

### 4.7.4 | CXCR4 phosphorylation and CXCL12 expression

To detect CXCR4 phosphorylation, cell pellets were resuspended in the primary antibody, namely CXCR4 (Ser339) Polyclonal Antibody from R&D systems at 0.02 µg/mL for 30 min in the dark at room temperature (as recommended by the manufacturer). To detect CXCL12 expression, cell pellets were resuspended in the primary antibody, namely SDF1 Polyclonal Antibody, from R&D Systems at 0.0135 mg/mL for 30 min (as recommended by the manufacturer). After 30 minutes, all samples were centrifuged at 504 x *g* for 3 min, washed once in 0.5% BSA in PBS buffer and centrifuged again at 504 x *g* for 3 min. The secondary antibody, namely Alexa Fluor 488 goat, was added to all samples at a concentration of 5 µg/mL for 30 min in the dark at room temperature, as per the manufacturer's instructions. After 30 minutes, cells were centrifuged at 504 x *g* for 3 min and resuspended in 0.5% BSA in PBS buffer.

## 4.8 | Compliance with ethical standards

Ethical approval for this study was obtained from the University of Pretoria, Faculty of Health Science, Research Ethics Committee (reference number: 405/2020).

## 4.9 | Statistics

All cytotoxicity experiments were done three times in triplicate. A minimum of four repeats were conducted for flow cytometry experiments. All quantitative data was represented as mean ± SEM. Data was checked for normality using the Shapiro–Wilks test and further tested for significant differences using one-way ANOVA with the Tukey test (if data was parametric) or the Kruskal–Wallis ANOVA with

the Dunn test (if data was non-parametric). $p \leq 0.05$ was considered significant.

## ACKNOWLEDGEMENTS

The authors acknowledge Ms Antoinette Lensink at the Electron Microscope Unit at the University of Pretoria. The author(s) disclose receipt of the following financial support for the research, authorship and/or publication of this article: The Research Development program of Dr YN Hlophe and Dr JC Serem by the University of Pretoria. Struwig/Germeshuysen Kankernavorsingstrust and School of Medicine Research Committee (RESCOM) Grant awarded to Ms Basson. National Research Foundation (NRF) awarded to Prof R Anguelov and Dr Hlophe.

## DATA AVAILABILITY STATEMENT

The dataset(s) supporting the conclusions of this article is(are) included within the article.

## ORCID

*Charlise Basson* https://orcid.org/0000-0002-6123-9707
*Avulundiah Edwin Phiri* https://orcid.org/0000-0001-9794-5438
*Manjunath Gandhi* https://orcid.org/0000-0001-7291-1151
*Roumen Anguelov* https://orcid.org/0000-0001-5456-0466
*June Cheptoo Serem* https://orcid.org/0000-0001-9912-166X
*Priyesh Bipath* https://orcid.org/0000-0002-5433-7069
*Yvette Nkondo Hlophe* https://orcid.org/0000-0002-3112-2436

## REFERENCES

1. Nkandeu DS, Basson C, Joubert AM, et al. The involvement of a chemokine receptor antagonist CTCE-9908 and kynurenine metabolites in cancer development. *Cell Biochem Funct*. 2022;40:608-622. doi:10.1002/cbf.3731
2. Zbytek B, Carlson JA, Granese J, Ross J, Mihm MC Jr, Slominski A. Current concepts of metastasis in melanoma. *Expert Rev Dermatol*. 2008;3:569-585. doi:10.1586/17469872.3.5.569
3. Saginala K, Barsouk A, Aluru JS, Rawla P, Barsouk A. Epidemiology of melanoma. *Med Sci (Basel)*. 2021;9:63. doi:10.3390/medsci9040063
4. Davis LE, Shalin SC, Tackett AJ. Current state of melanoma diagnosis and treatment. *Cancer Biol Ther*. 2019;20:1366-1379. doi:10.1080/15384047.2019.1640032
5. Davey MG, Miller N, McInerney NM. A review of epidemiology and cancer biology of malignant melanoma. *Cureus*. 2021;13:e15087. doi:10.7759/cureus.15087
6. Basson C, Serem JC, Bipath P, Hlophe YN. Chemokines as possible therapeutic targets in metastatic melanoma. *Cancer Med*. 2023a;12:14387-14402. doi:10.1002/cam4.6055
7. Müller A, Homey B, Soto H, et al. Involvement of chemokine receptors in breast cancer metastasis. *Nature*. 2001;410:50-56. doi:10.1038/35065016
8. Domanska UM, Kruizinga RC, Nagengast WB, et al. A review on CXCR4/CXCL12 axis in oncology: no place to hide. *Eur J Cancer*. 2013;49:219-230. doi:10.1016/j.ejca.2012.05.005
9. Busillo JM, Benovic JL. Regulation of CXCR4 signaling. *Biochim Biophys Acta*. 2007;1768:952-963. doi:10.1016/j.bbamem.2006.11.002
10. Huang EHMD, Singh BPD, Cristofanilli MMD, et al. A CXCR4 antagonist CTCE-9908 inhibits primary tumor growth and metastasis of breast cancer 1. *J Surg Res*. 2009;155:231-236. doi:10.1016/j.jss.2008.06.044
11. Anguelov R, Manjunath G, Phiri AE, et al. Quantifying assays: inhibition of signalling pathways of cancer. *Math Med Biol*. 2023;40:266-290. doi:10.1093/imammb/dqad005
12. Kim SY, Lee CH, Midura BV, et al. Inhibition of the CXCR4/CXCL12 chemokine pathway reduces the development of murine pulmonary metastases. *Clin Exp Metastasis*. 2008;25:201-211. doi:10.1007/s10585-007-9133-3
13. Pozdeyev N, Yoo M, Mackie R, Schweppe RE, Tan AC, Haugen BR. Integrating heterogeneous drug sensitivity data from cancer pharmacogenomic studies. *Oncotarget*. 2016;7:51619-51625. doi:10.18632/oncotarget.10010
14. Zhou W, Guo S, Liu M, Burow ME, Wang G. Targeting CXCL12/CXCR4 axis in tumor immunotherapy. *Curr Med Chem*. 2019;26:3026-3041. doi:10.2174/0929867324666170830111531
15. De Falco V, Guarino V, Avilla E, et al. Biological role and potential therapeutic targeting of the chemokine receptor CXCR4 in undifferentiated thyroid cancer. *Cancer Res*. 2007;67:11821-11829. doi:10.1158/0008-5472.CAN-07-0899
16. Juarez J, Bradstock KF, Gottlieb DJ, Bendall LJ. Effects of inhibitors of the chemokine receptor CXCR4 on acute lymphoblastic leukemia cells in vitro. *Leukemia*. 2003;17:1294-1300. doi:10.1038/sj.leu.2402998
17. Wong D, Kandagatla P, Korz W, Chinni SR. Targeting CXCR4 with CTCE-9908 inhibits prostate tumor metastasis. *BMC Urol*. 2014;14:12. doi:10.1186/1471-2490-14-12
18. Ullah TR. The role of CXCR4 in multiple myeloma: Cells' journey from bone marrow to beyond. *J Bone Oncol*. 2019;17:100253. doi:10.1016/j.jbo.2019.100253
19. Yu X, Huang Y, Collin-Osdoby P, Osdoby P. Stromal cell-derived factor-1 (SDF-1) recruits osteoclast precursors by inducing chemotaxis, matrix metalloproteinase-9 (MMP-9) activity, and collagen transmigration. *J Bone Miner Res*. 2003;18:1404-1418. doi:10.1359/jbmr.2003.18.8.1404
20. Appelqvist H, Wäster P, Kågedal K, Öllinger K. The lysosome: from waste bag to potential therapeutic target. *J Mol Cell Biol*. 2013;5:214-226. doi:10.1093/jmcb/mjt022
21. Kwong J, Kulbe H, Wong D, Chakravarty P, Balkwill F. An antagonist of the chemokine receptor CXCR4 induces mitotic catastrophe in ovarian cancer cells. *Mol Cancer Ther*. 2009;8:1893-1905. doi:10.1158/1535-7163.MCT-08-0966
22. Tavor S, Eisenbach M, Jacob-Hirsch J, et al. The CXCR4 antagonist AMD3100 impairs survival of human AML cells and induces their differentiation. *Leukemia*. 2008;22:2151-2158. doi:10.1038/leu.2008.238
23. Elmore S. Apoptosis: a review of programmed cell death. *Toxicol Pathol*. 2007;35:495-516. doi:10.1080/01926230701320337
24. Shaiken TE, Opekun AR. Dissecting the cell to nucleus, perinucleus and cytosol. *Sci Rep*. 2014;4:4923. doi:10.1038/srep04923
25. Chen Y, Henson ES, Xiao W, et al. Tyrosine kinase receptor EGFR regulates the switch in cancer cells between cell survival and cell death induced by autophagy in hypoxia. *Autophagy*. 2016;12:1029-1046. doi:10.1080/15548627.2016.1164357
26. Salazar M, Hernández-Tiedra S, Torres S, Lorente M, Guzmán M, Velasco G. Detecting autophagy in response to ER stress signals in cancer. *Methods Enzymol*. 2011;489:297-317. doi:10.1016/B978-0-12-385116-1.00017-0
27. Xu C, Zhao H, Chen H, Yao Q. CXCR4 in breast cancer: oncogenic role and therapeutic targeting. *Drug Des Devel Ther*. 2015;9:4953-4964. doi:10.2147/DDDT.S84932
28. Mebratu Y, Tesfaigzi Y. How ERK1/2 activation controls cell proliferation and cell death: is subcellular localization the answer? *Cell Cycle*. 2009;8:1168-1175. doi:10.4161/cc.8.8.8147
29. Zhao R, Liu J, Li Z, Zhang W, Wang F, Zhang B. Recent advances in CXCL12/CXCR4 antagonists and Nano-based drug delivery systems for cancer therapy. *Pharmaceutics*. 2022;14:1541. doi:10.3390/pharmaceutics14081541

30. Marampon F, Ciccarelli C, Zani BM. Biological rationale for targeting MEK/ERK pathways in anti-cancer therapy and to potentiate tumour responses to radiation. *Int J Mol Sci*. 2019;20:2530. doi:10.3390/ijms20102530
31. Persaud AK, Nair S, Rahman MF, et al. Facilitative lysosomal transport of bile acids alleviates ER stress in mouse hematopoietic precursors. *Nat Commun*. 2021;12:1248. doi:10.1038/s41467-021-21451-6
32. Berning P, Schaefer C, Clemens D, Korsching E, Dirksen U, Potratz J. The CXCR4 antagonist plerixafor (AMD3100) promotes proliferation of Ewing sarcoma cell lines in vitro and activates receptor tyrosine kinase signaling. *Cell Commun Signal*. 2018;16:21. doi:10.1186/s12964-018-0233-2
33. Couto GK, Segatto NV, Oliveira TL, Seixas FK, Schachtschneider KM, Collares T. The melding of drug screening platforms for melanoma. *Front Oncol*. 2019;9:512. doi:10.3389/fonc.2019.00512
34. Kong L, Smith W, Hao D. Overview of RAW264.7 for osteoclastogenesis study: phenotype and stimuli. *J Cell Mol Med*. 2019;23:3077-3087. doi:10.1111/jcmm.14277
35. Basson C, Serem JC, Hlophe YN, Bipath P. An in vitro investigation of L-kynurenine, quinolinic acid, and kynurenic acid on B16 F10 melanoma cell cytotoxicity and morphology. *Cell Biochem Funct*. 2023b; 41:912-922. doi:10.1002/cbf.3843
36. Kleeff J, Kornmann M, Sawhney H, Korc M. Actinomycin D induces apoptosis and inhibits growth of pancreatic cancer cells. *Int J Cancer*. 2000; 86:399-407. doi:10.1002/(sici)1097-0215(20000501)86:33.0.co;2-g

**How to cite this article:** Basson C, Phiri AE, Gandhi M, et al. In vitro effects and mathematical modelling of CTCE-9908 (a chemokine receptor 4 antagonist) on melanoma cell survival. *Clin Exp Pharmacol Physiol*. 2024;51(6):e13865. doi:10.1111/1440-1681.13865